

Review

# Progress in Short Wavelength Energy-Efficient High-Speed Vertical-Cavity Surface-Emitting Lasers for Data Communication

Si-Cong Tian <sup>1,2,\*</sup>, Mansoor Ahamed <sup>1,3</sup> and Dieter Bimberg <sup>1,2,\*</sup> <sup>1</sup> Bimberg Chinese-German Center for Green Photonics, Changchun Institute of Optics, Fine Mechanics and Physics, Chinese Academy of Sciences, Changchun 130033, China<sup>2</sup> Center of Nanophotonics, Institute of Solid State Physics, Technical University of Berlin, D-10632 Berlin, Germany<sup>3</sup> The University of Chinese Academy of Sciences, Beijing 100049, China

\* Correspondence: tiansicong@ciomp.ac.cn (S.-C.T.); bimberg@physik.tu-berlin.de (D.B.)

**Abstract:** The current progress of energy-efficient high-speed VCSELs based on GaAs substrates is presented. Novel approaches for the design of VCSELs are presented, potentially leading to larger bandwidth bit rates and lower power consumption. The first approach is based on the optimization of the VCSEL photon lifetime. The second one introduces a novel design based on oxidizing the apertures from multiple etched holes of varying geometries. These designs are also essential for improving the energy efficiency of future modules by optimizing the match of the electronic driver and the photonic device.

**Keywords:** vertical-cavity surface-emitting lasers (VCSELs); high speed; energy efficiency; photon lifetime; heat extraction; multi-hole apertures; multi-aperture VCSELs

## 1. Introduction



**Citation:** Tian, S.-C.; Ahamed, M.; Bimberg, D. Progress in Short Wavelength Energy-Efficient High-Speed Vertical-Cavity Surface-Emitting Lasers for Data Communication. *Photonics* **2023**, *10*, 410. <https://doi.org/10.3390/photonics10040410>

Received: 20 February 2023

Revised: 19 March 2023

Accepted: 23 March 2023

Published: 6 April 2023



**Copyright:** © 2023 by the authors. Licensee MDPI, Basel, Switzerland. This article is an open access article distributed under the terms and conditions of the Creative Commons Attribution (CC BY) license (<https://creativecommons.org/licenses/by/4.0/>).

Internet traffic increases by approximately 60% per year, much more than predicted from 2017 to 2022, 6 years ago [1]. Novel or more rapidly than expected expanding consumer and social media applications, such as Netflix and Block Chain, are responsible for this growth. The electrical power and cooling demands inside data centers are thus exploding. The introduction of 5G and the transition to 6G and the use of artificial intelligence (AI) and automotive applications will lead to further significant increases in the number, size, and power consumption of data centers. The objectives of this current research on optical interconnects being responsible for 80% to 90% of the power consumption of data centers must be supplemented by making energy efficiency, on all distance levels, a top priority, rather than just looking for higher bit rates at the expense of energy consumption. The introduction of limits for data consumption for the consumer must be prevented.

Vertical-cavity surface-emitting lasers (VCSELs) were becoming the dominating optical sources for data communication in such centers for all distances and wavelengths. VCSELs are of low production cost, can be tested on-wafer, and enable low energy consumption [2]. Presently, 850 nm multi-mode VCSELs are widely used for the optical links inside data centers and supercomputers, together with multi-mode fibers [3–5]. Long-wavelength single-mode VCSELs (1310 nm or 1550 nm) based on InP extend the transmission distance and enable wavelength division multiplexing (WDM) technologies.

GaAs-based VCSELs exhibit low threshold currents, large quantum efficiency, modulation frequencies up to 30 GHz, and a bit rate dependent on energy consumption [6]. An increase of line rates under non-return-to-zero on-off keying (NRZ-OOK) modulation and 4-level pulse amplitude modulation (PAM 4), including pre-emphasis, were demonstrated [7–9]. Using WDM, the optical link capacity can be greatly increased [10]. Low threshold currents and a large slope efficiency due to the small cavity volume, enables data transmission with a dissipated heat energy per bit of 56 fJ at a bit rate of 25 Gb/s [11]. The

present challenge is to achieve data transmission rates of 400 Gb/s and beyond at an energy per bit still less than 100 fJ/bit, for both short and long distances [12].

In this paper, we review the recent progress of energy-efficient high-speed VCSELs with wavelengths from 850 nm to 1060 nm. It is organized as follows: In Chapter 2, we will discuss the design approaches for energy-efficient high-speed VCSELs combined with wavelength multiplexing. In Chapter 3, we will review selected results based on conventional design, bit rate, and energy consumption. In Chapters 4 and 5, we will introduce novel designs approaches, including system design adapted photon lifetime tuning and aperture formation from multiple etched holes, enabling future generations of high-power multiple single-mode VCSELs. In Chapter 6, we will present a summary.

## 2. Energy Efficiency of High-Speed VCSELs

The electrical energy-to-data ratio (EDR) (fJ/bit), the dissipated heat-to-bit rate ratio (HBR) (fJ/bit), and the energy to data-distance ratio (EDDR) (fJ/(bit·km)) were defined in previous works [13,14]. Such definitions are essential in comparing the power consumption of different VCSEL designs.

$$\text{EDR} = \frac{P_{el}}{\text{BR}} \quad (1)$$

$$\text{HBR} = \frac{P_{diss}}{\text{BR}} \quad (2)$$

$$\text{EDDR} = \frac{P_{el}}{(\text{BR} \cdot d)} \quad (3)$$

where  $P_{el} = V \cdot I$  (mW) is the CW bias power,  $V$  and  $I$  are the bias voltage and current,  $P_{diss} = P_{el} - P_{optical}$  (mW) is the power dissipated as heat,  $P_{optical}$  (mW) is the optical output power,  $\text{BR}$  (Gb/s) is the bit rate, and  $d$  (m) is the distance.

The modulation energy per bit needs to be added to the EDR to calculate the total energy consumption per bit of a module. The modulation energy dissipated in the VCSEL can be determined by the root mean square (RMS) power  $P_{BPG}$ , which is provided by the bit pattern generator (BPG) at a given modulation peak-to-peak voltage,  $V_{pp}$ , and the bit rate. The impedance of VCSELs typically does not match the 50-Ω impedance of a probe A portion of the power is reflected and does not contribute to the generation of photons. The amplitude reflection coefficient  $r$  is calculated as:

$$r = \frac{Z_A - Z_L}{Z_A + Z_L} \quad |r| \leq 1 \quad (4)$$

where  $Z_A$  and  $Z_L$  are the impedance of the VCSEL and the impedance of the transmission line, respectively.  $Z_A$  and  $Z_L$  are a function of frequency. Mostly, the  $Z_L$  of the standard high-frequency transmission lines is 50 Ω. The impedance  $Z_A$  is approximated by the differential resistance  $R_d$  ( $I$ ) at the bias current used in the data transmission experiment. The fraction of the power, which is reflected because of the mismatch of the impedance, is given by  $|r|^2$ .

By adding the modulation power dissipated in the VCSEL to the EDR defined in (1), one can obtain the  $\text{EDR}_{\text{mod}}$ :

$$\text{EDR}_{\text{mod}} = \frac{V \cdot I}{\text{BR}} + \frac{P_{BPG}}{\text{BR}} (1 - |r|^2) \quad (5)$$

where  $P_{BPG}$  is the power provided by the bit pattern generator (BPG),  $1 - |r|^2$  is the fraction of the power  $P_{BPG}$  entering the VCSEL.  $\text{HBR}_{\text{mod}}$  can be obtained by:

$$\text{HBR}_{\text{mod}} = \frac{V \cdot I - P_{optical}}{\text{BR}} + \frac{P_{BPG}}{\text{BR}} (1 - |r|^2) (1 - \text{WPE}(I)) \quad (6)$$

where  $\text{WPE}(I)$  is the static wall plug efficiency (WPE) of the VCSEL, and  $I$  is the bias current used in the data transmission experiment. In addition,  $(1 - |r|^2)(1 - \text{WPE}(I))$  is the fraction of the power  $P_{\text{BPG}}$ , which enters the VCSEL, but is turned into heat and thus does not contribute to the creation of photons.

However, a VCSEL design for optimizing the WPE may deteriorate the dynamic performance of the VCSEL, resulting in a larger energy consumption for error-free data transmission. VCSELs with a smaller WPE can be more energy efficient compared to VCSELs with larger WPEs. In addition, the current at which the WPE is maximum is not necessarily the same current at which the highest energy efficiency of the VCSEL is achieved. Thus, WPE alone is an important but not sufficient indicator of low energy consumption per bit. The static, as well as the dynamic, properties of a VCSEL must be evaluated at the same time to draw proper conclusions about the energy efficiency of the device.

By using the HBR and EDR, the WPE can be derived as:

$$\text{WPE} = 1 - \text{HBR}/\text{EDR} \quad (7)$$

In order to achieve a large energy efficiency, the electrical power  $P_{el}$  should be low and the BR should be large. By assuming that the current is linearly related to the voltage above threshold, the electrical power  $P_{el}$  can be calculated by the following equation:

$$P_{el} = U_{th} \cdot I_{th} + R_{d,th}(I - I_{th})^2 \quad (8)$$

where  $U_{th}$  is the threshold voltage,  $I_{th}$  is the threshold current, and  $R_{d,th}$  is the differential resistance at  $I_{th}$ . These three parameters all depend on the volume of the active region of the VCSEL. In GaAs-based VCSELs, the oxide aperture is typically used for the confinement of the emitted light and the current. The volume of the active region of an oxide-confined VCSEL is the product of the aperture area and the thickness of the active material. VCSELs with small oxide-aperture diameters have small  $U_{th}$  and  $I_{th}$ , but large  $R_d$ . Because of the large  $R_d$ , the driver power is typically larger at a given current for VCSELs with a small oxide aperture compared to ones with a large aperture.

The single-mode density-rate equations describe the change of the charge carrier and the photon densities inside the VCSEL with time. The dependence of the charge carrier density  $N$  and photon density  $N_p$  on the time is:

$$\frac{d}{dt}N = \frac{\eta_i I}{qV} - (R_{sp} + R_{nr} - v_g g N_p) \quad (9)$$

$$\frac{d}{dt}N_p = \left( \Gamma v_g g - \frac{1}{\tau_p} \right) N_p + \Gamma R'_{sp} \quad (10)$$

where  $\eta_i$  is the internal quantum efficiency,  $I$  is the bias current,  $V$  is the volume of the active region,  $q$  is the elementary charge,  $R_{sp}$  and  $R_{nr}$  are the spontaneous and non-radiative recombination rates,  $v_g$  is the photon group velocity,  $g$  is the optical gain,  $\tau_p$  is the photon lifetime,  $\Gamma$  is the optical confinement factor, and  $R'_{sp}$  is the rate of the spontaneous emission that emits into the laser mode. Gain compression is accounted for in  $g = g_0 / (1 + \varepsilon \cdot N_p)$ , where  $g_0$  is the gain coefficient, and  $\varepsilon$  is the empirical gain compression factor. Therefore,  $g$  is nonlinearly dependent on  $N_p$ .

To analyze the small-signal frequency of VCSEL, we assume there is a small sinusoidal modulating current with an amplitude of  $I_1$  superimposed on the steady-state bias current  $I_0$ . Then, we have:

$$I(t) = I_0 + I_1 e^{i\omega t} \quad (11)$$

$$N(t) = N_0 + N_1 e^{i\omega t} \quad (12)$$

$$N_p(t) = N_{p0} + N_{p1}e^{i\omega t} \quad (13)$$

where  $N_0$  and  $N_{p0}$  are the steady-state carrier and photon densities,  $N_1$  and  $N_{p1}$  are the corresponding small-signal modulation amplitudes, and  $\omega$  is the angular frequency. Substituting Equations (11)–(13) into Equations (9) and (10), neglecting the products of the small-signal terms but retaining other first-order deviations, the modulation transfer function is obtained:

$$H_{\text{int}}(\omega) = A_i \frac{\omega_r^2}{(\omega_r^2 - \omega^2 + i\omega\gamma)} \quad (14)$$

where  $A_i$  is the DC slope efficiency,  $\omega_r$  is the relaxation resonance frequency, and  $\gamma$  is the damping factor. The setting is  $f_r = \omega_r/2\pi$  and, using the method in Ref. [15], the value of the relaxation resonance frequency is  $f_r$  and the damping  $\gamma$  can be expressed as follows:

$$f_r = D \sqrt{I - I_{th}} \quad (15)$$

$$\gamma = K f_r^2 + \gamma_0 \quad (16)$$

where  $D$  and  $K$  are the D-factor and K-factor, respectively,  $I_{th}$  is the threshold current of the VCSEL, and  $\gamma_0$  is the damping offset.  $D$  and  $K$  can be expressed as:

$$D = \frac{1}{2\pi} \sqrt{\frac{\eta_i \Gamma v_g}{q V_a} \frac{\partial g / \partial n}{\chi}} \quad (17)$$

$$K = 4\pi^2 \left( \tau_p + \varepsilon \frac{\chi}{v_g (\partial g / \partial n)} \right) \quad (18)$$

where  $\partial g / \partial n$  is the differential gain, and  $\chi$  is the transport factor.

To realize a large intrinsic modulation bandwidth of VCSELs, a large D-factor and a reasonably low K-factor are needed. In addition, the modulation bandwidth of VCSELs is also affected by the thermal and parasitic effects. Therefore, high-speed VCSELs need to be designed by optimizing intrinsic modulation speed, heat dissipation, and parasitics [2].

VCSELs with a small oxide-aperture diameter have a larger D-factor because of the small volume of the active region as compared to VCSELs with a larger oxide-aperture diameter. Then, the current-induced self-heating is large, leading to large damping, and consequently, the maximum achievable BR is small.

Additionally,  $f_r$  is proportional to the square root of the current above threshold, and therefore, VCSELs consume more energy at a larger BR. Equation (15) is valid until  $f_r$  saturates, when the current reaches rollover. Thus, in order to operate VCSELs energy efficiently, the BR must be lower than the maximum achievable BR. VCSELs emitting between 850 and 1060 nm with oxide-aperture diameters from 4 to 7  $\mu\text{m}$  can have the highest BRs. The low damping of these devices enables large bandwidths via increasing the bias current. Adapting the reflectivity of the top DBR, and thus the photon lifetime, is the best tool for manipulating the damping of VCSELs [16,17].

The dependence of the D-factor and the K-factor suggests that VCSELs with smaller oxide-aperture diameters (larger than 2  $\mu\text{m}$ ) can have higher energy efficiencies than ones with larger oxide-aperture diameters. When the oxide-aperture diameter reaches 2  $\mu\text{m}$ , the increased self-heating and optical diffraction losses result in the overall performance degradation of the VCSEL. To benefit from the larger D-factor of VCSELs with small oxide apertures, the VCSELs need to be operated at small currents, where the damping is dominated by the small damping offset.

The experimentally measured maximum bit rate at the given bias current at which the VCSEL operates largely depends on the measurement setup. In order to better analyze the energy efficiency of a VCSEL, and to account for the influence of the system in which the

VCSEL is incorporated, BR is replaced by the product of the  $-3$  dB small-signal modulation bandwidth ( $f_{3dB}$ ) and the modulation factor  $M$  in units of (b/s)/Hz.

$$\text{EDR} = P_{el} / (M \cdot f_{3dB}) \quad (19)$$

$$\text{HBR} = P_{diss} / (M \cdot f_{3dB}) \quad (20)$$

The error-free bit rate of a VCSEL is related to  $f_{3dB}$  and depends on the measurement system. Thus,  $M$  describes the overall optical interconnect (OI) system, whereas the electrical power and  $f_{3dB}$  reflect the intrinsic properties of the VCSEL. Due to the improvements of high speed detectors and receivers, the typical  $M$ -factor has been increasing. Higher order modulation formats, such as PAM 4, can also be modeled by using a representative  $M$ -factor.

Even though these considerations are generally independent of the laser wavelength, the desired emission wavelength also impacts the potential maximum bit rate. The devices with a wavelength of 980–1060 nm, for example, employing lower energy bandgap active region materials (quantum wells (QWs) or quantum dots (QDs)), provide superior carrier confinement, making them more stable at elevated temperatures.

Figure 1 gives an overview of the presently dominating VCSEL technologies. For VCSELs with wavelengths from 850 to 1060 nm, mostly strained InGaAs QWs based on GaAs substrates are used, enabling large differential gains due to strain-induced valence band splitting [18]. Ternary or still binary DBRs with a large contrast of the index of refraction of the layers are easily grown on GaAs substrates [19]. The oxide apertures are used to confine the light and the current and to lower the device's capacitance to decrease the parasitics effect on the cutoff frequency of the VCSEL [20].

For long wavelength VCSELs, with the wavelengths of 1310 and 1550 nm, the strained InGaAs QWs based on InP substrates are used to achieve a large differential gain [21,22]. The buried tunnel junction (BTJ) are used to confine the light and the current and to lower the resistance of the device, so as to decrease the parasitics effect on the cutoff frequency of the VCSEL [23–25]. However, the ternary DBR, based on InP substrates, need more pairs of DBR to have enough confinement because of the low difference of the index value, and so many pairs of the DBR together with the Auger recombination will result to the problem of the heat extraction. The wafer-fusion technique of an InP-based optical cavity with a GaAs-based top and bottom Al(Ga)As/GaAs DBR is used to solve such a problem [21,26].

850 nm ... 980 nm ... 1310 nm ... 1550 nm		
Gain	strained InGaAs MQW on GaAs	strained InGaAs MQW on InP
$\Gamma_{\text{confinement}}$	DBR on GaAs	DBR on InP or GaAs
Parasitics	low $C$ : Oxide Apertures	low $R$ : Tunnel Junct. or intracavity contacts
Heat extraction	ternary /	binary DBR on GaAs
		ternary DBR on InP or GaAs/AlAs (wafer fusion)

**Figure 1.** Present device technologies for the 850–1550 nm wavelength window [27]. For longer wavelengths, GaSb-based material structures are considered.

Table 1 summarizes the state of the art of energy efficiency of high-speed VCSELs from 850 to 1550 nm in the last approximate 10 years.

**Table 1.** Energy Efficiencies of High-Speed VCSELs.

Group	$\lambda$ (nm)	BR (Gb/s)	Energy Eff. (fJ/bit)	Oxide Aperture/BTJ ( $\mu\text{m}$ )	Year	Refs.
TUB-VIS	850	25	EDR 77HBR 56	3.5	2012	[11]
TUB	850	40	HBR 108	4	2013	[28]
TUB	850	30 25	HBR 85@500 mHBR 100@1000 m	3	2013	[13]
CUT	850	50	HBR 95	3.5	2015	[29]
UIUC	850	40	EDR 431	4	2014	[30]
NCU	850	34	EDR 140HBR 107	4	2013	[31]
TUB	980	38	HBR 177@85 °C	5.5	2014	[32]
TUB	980	50	HBR 302	5	2014	[33]
CUT	1060	50	HBR 100	4	2017	[34]
Furukawa	1060	25	HBR 76	5	2011	[35]
TUM-TUB	1300	25	EDR 270@10 km	3	2012	[36]
TUB-EPFL	1300	38	EDR 797@PAM4	6	2017	[37]
TUM	1550	50	HBR 130	4	2017	[38]

### 3. Energy-Efficient High-Speed Short-Wavelength VCSELs

#### 3.1. 850 nm VCSELs

Presently, 850 nm MM VCSELs are the main light source for short distance optical interconnects (less than 300 m) because of their low cost. In early work, unstrained GaAs QWs with AlGaAs barrier layers were used for 850 nm high-speed VCSELs. In more recent work, strained InGaAs QWs were adopted because of their larger differential gain, compared to unstrained GaAs QWs. Many groups have realized up to an approximate 30 GHz modulation bandwidth of 850 nm VCSELs, by using strained InGaAs QWs, in combination with graded interfaces and modulation doped DBRs, multiple oxide apertures, a short cavity, and photon lifetime tuning [29,39,40]. Under both NRZ-OOK (PAM 2) and PAM 4 modulation, the bit rates for short distances have been increased beyond 50 Gb/s or 100 Gb/s, respectively. Larger link capacities are achieved using feed-forward equalization (FFE) [8,41].

Bimberg's group realized the largest bit rates for error-free data transmission combined with the lowest energy consumption for 850 nm VCSELs [11,42]. The schematic cross-section of such an oxide-confined VCSEL is shown in Figure 2. The VCSEL was formed by 21 pairs of *p*-doped Al<sub>0.12</sub>Ga<sub>0.88</sub>As/Al<sub>0.90</sub>Ga<sub>0.10</sub>As top DBR, 33.5 pairs of *n*-doped Al<sub>0.12</sub>Ga<sub>0.88</sub>As/Al<sub>0.90</sub>Ga<sub>0.10</sub>As bottom DBR and an active region of five 12-monolayers-thick strained In<sub>38</sub>Ga<sub>62</sub>As QWs, surrounded by Al<sub>0.45</sub>Ga<sub>0.55</sub>As barrier layers. Multiple oxide layers were employed to reduce the capacitance of the VCSEL. Compared to the design in Refs. [13,14], this design has a larger mole fraction of indium, thinner QWs, and a thinner overall active area. This approach is beneficial to reduce the transit time, suppress vertical carrier leakage, increase the confinement of photons in the cavity, and thus improve the modulation response. Modulation doping was adopted throughout both DBRs to minimize the absorption losses and increase the efficiency. A highly *p*-doped GaAs phase-offset layer was added on the topmost DBR to act as a low contact resistance layer in addition to a photon lifetime tuning layer.

For VCSELs with oxide-aperture diameters of 3.5  $\mu\text{m}$ , error-free data transmission at 25 Gb/s with the record low EDR of 77 fJ/bit and HBR of 56 fJ/bit was realized [11,42], as shown in Figure 3. The current density for achieving a 25-Gb/s operation was below 10 kA/cm<sup>2</sup>, demonstrating the suitability of such devices for applications in highly reliable commercial OI systems. Larger bit rates were achieved based on the same design. For

40 Gb/s, an HBR of 108 fJ/bit was demonstrated [28]. Error-free data transmission at 30 Gb/s across 500 m of MMF was realized with an HBR of 85 fJ/bit. Additionally, at 25 Gb/s across 1000 m of MMF, an HBR of 100 fJ/bit was demonstrated [29]. It was demonstrated that the smaller oxide-aperture-diameters VCSELs are more energy efficient than the ones with larger aperture diameters, due to the large D-factor of the small oxide aperture (shown in Figure 4).

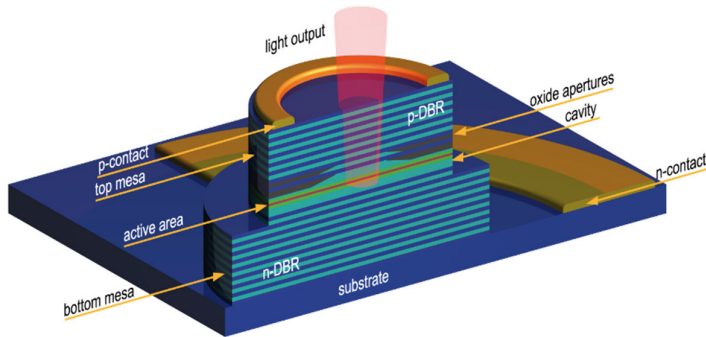


**Figure 2.** Schematic cross-section of oxide-confined VCSELs [43].

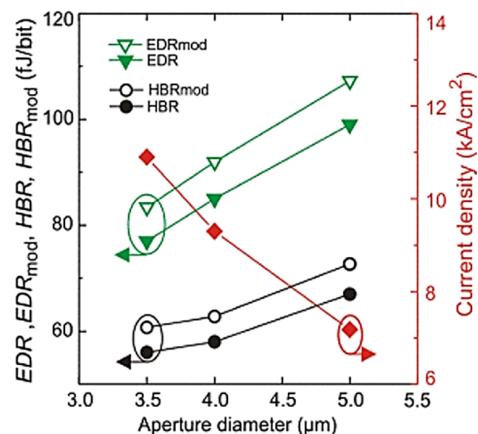


**Figure 3.** EDR, HBR, EDR<sub>mod</sub>, HBR<sub>mod</sub>, and current density at error-free 25 Gb/s operation versus the oxide-aperture diameter [42].

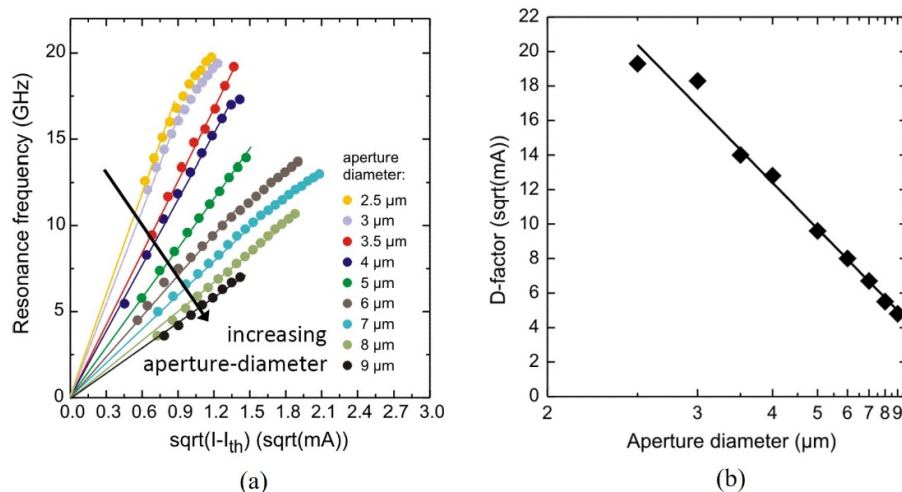


**Figure 4.** (a) Relaxation resonance frequency versus the square root of the current above the threshold current for 850 nm VCSELs with aperture diameters ranging from 2.5 to 9  $\mu\text{m}$ . The straight lines indicate the linear fits to obtain the D-factors. (b) D-factors versus the aperture diameters of 850 nm VCSELs [42].

Alternatively to oxide apertures, Zn-diffusion and oxide-relief techniques were reported to be successful in Ref. [31].

### 3.2. 980 nm and 1060 nm VCSELs

High-speed VCSELs with wavelengths from 980 to 1100 nm have attracted a lot of attention recently, although they are not yet included in the standards of IEEE [44]. Compared with 850 nm high-speed VCSELs, devices emitting at longer wavelengths benefit from lower chromatic dispersion and lower transmission loss in MMF, and a larger temperature insensitivity of the quantum efficiency, due to reduced carrier spill-out of the well. Again, strained InGaAs QWs (or QDs) can be used to create emissions from 980 to 1100 nm. These QWs show a larger differential gain and lower transparency carrier density, allowing a larger D factor, and in turn, a larger modulation bandwidth. Work on high bit rate NRZ-OOK data transmission in MMF links was carried out for 980 to 1100 nm VCSELs [16,32–35,45,46]. At 980 nm, the TU Berlin group demonstrated a 46 Gb/s NRZ-OOK data transmission at 85 °C [33]. By optimizing the photon lifetime of 980 nm VCSELs, Larisch et al. increased the data rate to 50 + Gb/s at 85 °C [16], a number limited then by the measurement set-up.

Li et al., from Bimberg's group, realized error-free data transmission at 38 Gb/s at 85 °C, with a record low HBR of 177 fJ/bit by using 980 nm VCSELs [32]. The active region of the VCSEL was formed by five 4.2 nm-thick compressively strained  $In_{0.21}Ga_{0.79}As$  QWs surrounded by 6 nm  $GaAs_{0.12}P_{0.88}$  partially strained compensating barrier layers. The optical cavity thickness is  $1.5\lambda$ . A 15 nm QW gain-to-etalon wavelength offset was used to improve the VCSEL temperature stability, as well as to enable energy-efficient operation at high temperatures. Across the entire temperature range, the modulation peak-to-peak voltage was kept unchanged. In addition, temperature-stable energy dissipation was realized.

This design was improved later and a larger bit rate of 46 Gb/s was achieved at 85 °C. Compared with the previous design, the optical cavity thickness was reduced to  $\lambda/2$  to increase the photon density at the QWs. Five compressively strained 4 nm-thick  $In_{0.22}Ga_{0.78}As$  QWs with 5.1 nm-thick tensile-strained  $GaAs_{0.9}P_{0.1}$  barrier layers partially compensating the QW layer strain formed the active region. A total of 21.5 pairs of *p*-doped  $GaAs/Al_{0.90}Ga_{0.10}As$  top DBR and 35 pairs of *n*-doped bottom DBR mirrors, both including modulation-doped current spreading layers, were designed. Two 20 nm-thin oxide apertures, which were formed by the selective wet oxidation of  $Al_{0.98}Ga_{0.02}As$  layers, were used for optical and current confinement. Additional GaAs layers were added to the topmost DBR for the purpose of the photon lifetime tuning. Error-free operation at 50 Gb/s at 25 °C was achieved for the 5 μm oxide-aperture diameter VCSELs. At this bit rate, the HBR was 302 fJ/bit, which was lower than the value of 340 fJ/bit for 850 nm VCSELs. Error-free operation at 46 Gb/s at 85 °C was also achieved, due to a 16 nm QW gain-to-etalon wavelength offset [33].

Simpanen et al. realized energy-efficient high-speed 1060 nm VCSEL using a design derived from their previous 850 nm VCSEL [34]. Five strained InGaAs QWs were used as the active region to achieve high differential gain. A half-wavelength-thick short cavity was used for large longitudinal optical confinement. Twenty  $Al_{0.9}Ga_{0.1}As/GaAs$  top *p*-doped DBRs with modulation-doped and parabolically graded compositional intermediate layers were adopted to have a low resistance and optical loss. Five pairs of  $Al_{0.9}Ga_{0.1}As/GaAs$  and 24 pairs of  $AlAs/GaAs$  bottom *n*-DBRs with modulation-doped and step-graded compositional intermediate were shown to have a low thermal impedance. Multiple oxide apertures were in the top DBR. The two primary oxide apertures provided transverse optical and current confinement, and the other four secondary oxide apertures reduced the capacitance. By using 4 μm oxide apertures, HDRs of 100 fJ/bit at 50 Gb/s NRZ-OOK modulation was reported for 1060 nm VCSELs.

Excellent energy efficiency for high-speed 1060 nm VCSELs was also achieved by Furukawa [35]. Oxide-confined double intra-cavity structures are used here. Compressively

strained InGaAs QWs provided high differential gain. Undoped semiconductor bottom-DBR and dielectric top-DBR were used, leading to low internal optical loss. For 5  $\mu\text{m}$  aperture VCSELs, a power dissipation of 76 fJ/bit at 25 Gb/s and 2 mA bias current was demonstrated.

#### 4. Adapt Photon Lifetime of VCSELs to Data Rate

In previous work, the impact of photon lifetime tuning on the performance of high-speed VCSELs was investigated. By etching the GaAs layer of the topmost DBR, the mirror loss was increased, thus the photon lifetime and the damping became smaller. Therefore, at a given electrical power,  $P_{el}$ , the VCSEL with an etched DBR achieved a larger  $f_{3\text{dB}}$ , compared with VCSELs without etched DBR. These results indicated that photon lifetime tuning does not only improve the static performance, such as the maximum output power, but can also improve the energy efficiency of the VCSEL [16], as shown in Figure 5, where SiN was deposited on top of the surface, instead of etching.

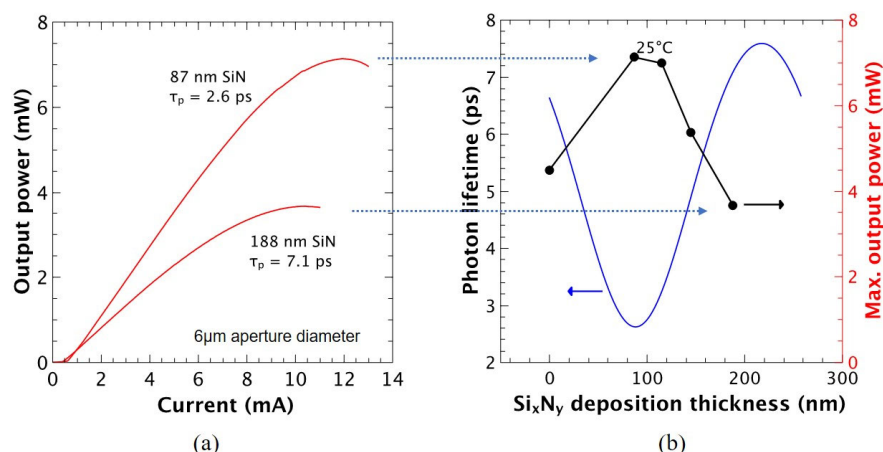


**Figure 5.** (a) Output power as a function of current of a 6  $\mu\text{m}$  oxide-aperture diameter VCSELs with different thicknesses of SiN and photon lifetimes. (b) Photon lifetime and max. output power of the VCSEL as a function of the thickness of SiN [16].

The tuning of the photon lifetime and damping of any VCSEL can be realized with large precision by the homogeneous deposition of SiN on the top layer, which can be better controlled than etching. The output power and the cut-off frequency of the VCSEL can be increased [47], and the energy consumption can be decreased by adapting the photon lifetime. Figure 6 shows experimental results for the EDR as a function of the bit rate for a long photon lifetime (blue curve) and a short photon lifetime (red curve) tuned by the deposition of SiN on the top DBR. The modulation current efficiency factor has been determined experimentally based on large signal measurement results marked with (a) and (c) for both photon lifetimes [16,33]. At 50 Gb/s, by using the VCSEL with long photon lifetime (large damping), the EDR is 530 fJ/bit, while by using the VCSEL with a short photon lifetime (small damping), the EDR is only 400 fJ/bit. Therefore, a 25% reduction of EDR is achieved for a 50 Gb/s data transmission by choosing the optimum photon lifetimes of the VCSELs. In addition, in Figure 6, a crossover between the two curves is observed. The grey dashed line passing through the crossing divides the two curves into two sections. From an energy-consumption point of view, it is preferable to fabricate VCSELs with a short photon lifetime at larger bit rates ( $>44 \text{ Gb/s}$ ), whereas it is advantageous to use long photon lifetimes at medium or lower bit rates. These results are important for the optimization of energy consumption, which is shown below.

It was demonstrated that drivers with forward error correction (FEC) and equalization, as well as higher order modulation formats like PAM 4, can increase the bit rates of optical links. However, the energy cost per bit for data transmission at larger bit rates needs to be compared with that of data transmission at lower bit rates using wavelength multiplexing

at the smaller rates, still achieving the same transmission capacity. Coarse wavelength division multiplexing (coarse WDM), which is standardized in Ethernet 802.3 bs and CEI-56G, is useful for putting energy consumption EDR optimization ideas into practice. The number of VCSELs used in a WDM system impacts more than only increasing the capacity of the optical link. Choosing the number of VCSELs provides a new degree of freedom for the optimization of the energy consumption for a target bit rate. Using VCSELs with wavelengths of 850 nm, 880 nm, 910 nm, and 940 nm, WDM for more than 200 Gb/s data transmission was demonstrated [10]. It is also possible to achieve a 200 Gb/s data transmission by switching to eight VCSELs, having a 15 nm wavelength difference and each operating at 25 Gb/s. By employing VCSELs with a short photon lifetime, the EDR at 50 Gb/s is 400 fJ/bit, whereas the EDR at 25 Gb/s is less than 100 fJ/bit by employing VCSELs with a long photon lifetime. Therefore, adaptive photon lifetime tuning, combined with WDM, can reduce energy consumption by more than 50% for the same 200 Gb/s optical link. Additionally, the decreased current density, up to 25 Gb/s operating conditions, results in less heat and lowers the possibility of device failure.

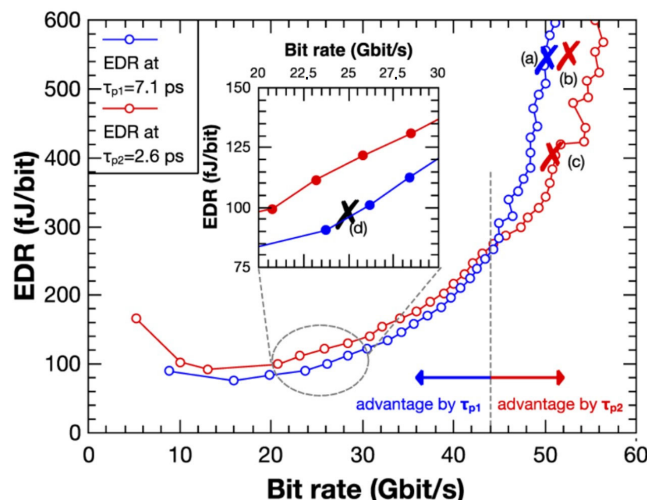
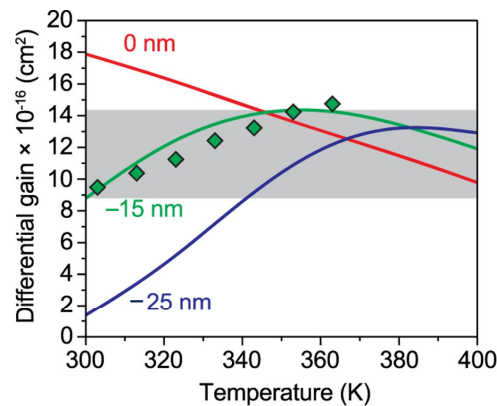


**Figure 6.** EDR and BR values from small signal measurements, for a long photon lifetime (blue) and a short photon lifetime (red). A spectral efficiency of  $M = 2.1$  bits was observed experimentally by the large signal measurements, marked with (a) and (c) for both photon lifetimes. The data points marked with (a), (b), and (c), as well as the curves, are achieved with the identical device. Datapoint (d) was measured with a different but similar aperture device [47].

The noise of the VCSELs dominates the noise of the whole link and determines the spectral efficiency. Increasing the photon lifetime will result in an increase in the K-factor, and thus the damping, and reduces the noise. VCSELs with long photon lifetimes are therefore advantageous for increasing spectral efficiency and are better suited for higher order modulation formats to increase the data rate.

##### 5. Novel Processing Approach for Aperture Formation Improving Heat Conduction and Reducing Series Resistance: The MuHA and MAV Designs

Our previous epitaxial structures were designed to have an off-set between the room temperature (RT) emission peak and the maximum transmission of the DBRs, which is called a gain-to-etalon wavelength off-set [48]. The emission peak at RT is positioned at a shorter wavelength in order to have a response extended to larger temperatures, as shown in Figures 7 and 8.



**gain-to-etalon wavelength offset** leads to:

- temperature insensitive differential gain
  - temperature stable operation, eliminating Peltier cooling
  - high speed both at room temperature and high temperatures
  - size of off-set determines max operating temperature

**Figure 7.** Differential gain versus temperature for 300 K gain-to-etalon wavelength offsets of 0,  $-15$ , and  $-25$  nm. The lines are calculated results based on 8-band  $k\cdot p$  theory, and the diamonds are experimental results extracted from small signal measurements of 980 nm VCSELs [48].

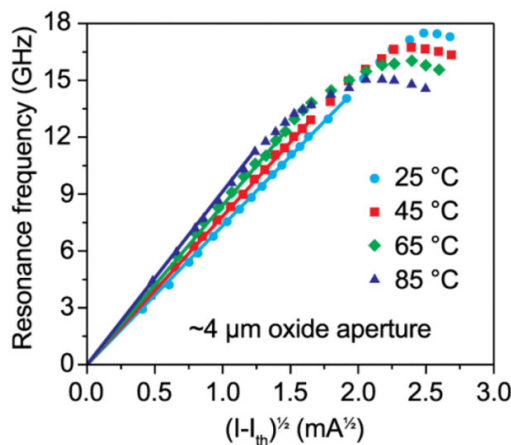


**Figure 8.** Relaxation resonance frequency versus square root of bias current minus threshold current for an approximate  $4.0\ \mu\text{m}$  oxide-aperture diameter VCSEL at 25, 45, 65, and 85 °C [48].

Therefore, for a larger temperature, such as 85 °C, the initial slope of the resonance frequency curves in Figure 8 is largest. However, it shows a lower maximum frequency and bends over at lower currents more so than the curves at lower temperatures. All resonance frequency curves for different temperatures show thermal roll-over at a different current. The largest resonance frequency at roll-over is achieved at RT. This systematic is easily understood: a slope quantum efficiency below 100% causes the temperature inside the active area to rise to values larger than the “test temperature” with rising current. The actual active area temperature depends on the heat dissipation of the structure.

We developed a novel processing approach to oxidize the apertures of VCSELs [49,50] leading to much better heat dissipation from the active area. A number of holes in a symmetric square, hexagonal, or an asymmetric arrangement, are etched into the epitaxial structure to a depth slightly below the layer to be oxidized, but still above the active area. Then the aperture(s) is/are oxidized from these holes. Therefore, practically any geometry for a single oxide aperture or several oxide apertures is feasible. After the oxidation, the bottom of the holes is covered with an insulator and then the holes are filled with metal.

Heat dissipation is predicted to be significantly improved, because the transport of phonons through the top mirror, with its *p*-doping and many phonon reflecting interfaces, is circumvented. In addition, the series resistance will be lowered because the current is injected via the metal-filled holes to the aperture(s) and the *p*-doped mirrors are at least partly circumvented. To achieve single mode emission, the aperture size of the classical VCSELs needs to be small, resulting in a large series resistance of several hundred Ohms. Typical drivers with low impedance are now suddenly matched to the VCSELs, presenting a break-through for the complete system. A significant step towards green photonics for a sustainable future can be presented by novel high-speed CMOS driver circuits, significantly reducing the energy consumption of the module.

SM VCSELs with high power are preconditioned for long-distance data transmission, enabling dense wavelength multiplexing based on existing fiber designs. The only way to obtain single mode emission and large cut-off frequencies is by using small oxide apertures. In comparison to large oxide-aperture VCSELs, which are multi-mode, small oxide-aperture VCSELs have a low power output and a larger series resistance. A revolutionary design concept called MuHA (multi-hole apertures) for novel types of single-mode high power VCSELs was presented above. A multi-aperture concept is based on the MuHA concept [51–53]. Figure 9 shows the schematic of MuHA VCSELs. Figure 10a–c depicts microscope photos of the top mesa of the MuHA VCSELs and multi-aperture VCSELs (MAVs). We fabricated the VCSELs in such way, that all the emissions can be easily coupled to MMFs with a 50- $\mu\text{m}$  diameter. Figure 10d shows hexagon-shape MAVs with seven apertures, the diameter of each aperture being 2.0  $\mu\text{m}$ , enabling a single-mode emission from each aperture. The current goes through all apertures, and the output light from all apertures is collected and measured as one device. The pitch size of aperture-to-aperture is presently around 15  $\mu\text{m}$ . Therefore, there is no optical leakage-induced interaction between the apertures allowing incoherent lasing. The processing of closer lying apertures is under way. Figure 11 shows NRZ-OOK data transmission at 40, 45, and 50 Gbit/s crossing 100 m-length MMF. The largest open-eye diagram is 60 Gbit/s, with the S/N better than 4 for a MAV testing one aperture. By improving some of our processing parameters, larger data transmission rates using MAV with multi-apertures are expected. Figure 12 shows a side mode suppression ratio of more than 40 dBm at all currents for one of the apertures of a four aperture MAV based on a hexagonal arrangement of holes.

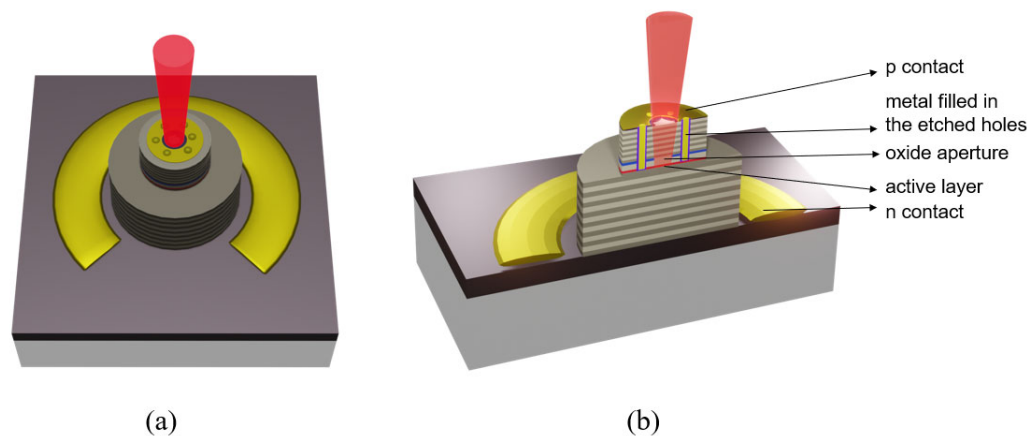


**Figure 9.** (a) Schematic of MuHA VCSELs. (b) Schematic cross-section of MuHA VCSELs.

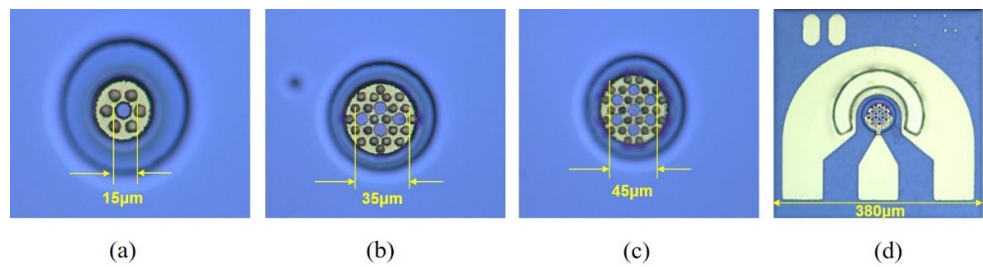


**Figure 10.** The microscope picture of the top mesa with (a) one aperture, (b) four apertures, and (c) seven apertures. (d) The microscope picture of the MAV with seven apertures. A number of holes are arranged in a symmetric hexagonal.

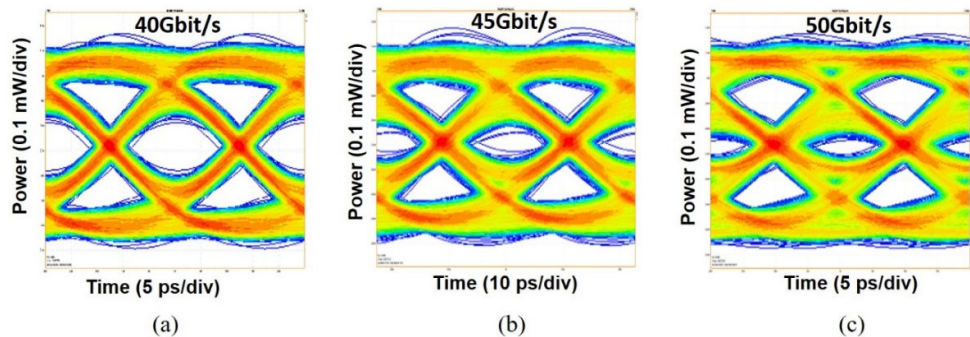
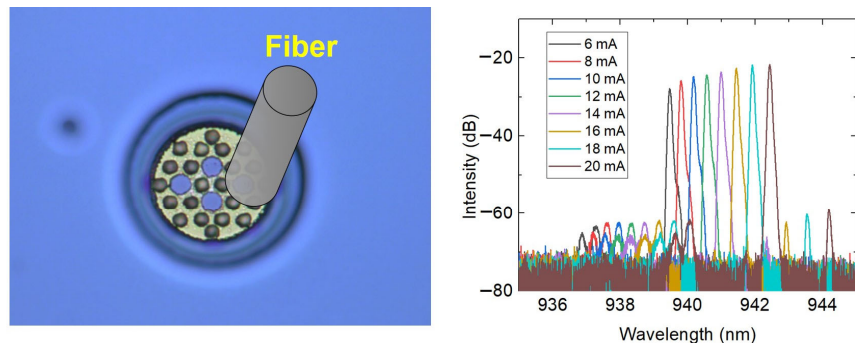


**Figure 11.** The eye diagram of hexagon-shape MAVs with seven 2.0- $\mu\text{m}$  apertures across a 100 m-length MMF, (a) 40 Gbit/s, (b) 45 Gbit/s, (c) 50 Gbit/s.



**For each aperture, the emission is single-mode, SMR larger than 40 dB**

**Figure 12.** Optical spectrum of one of the apertures of a four aperture MAV based on a hexagonal arrangement of holes.

Additional significant performance benefits are anticipated, including much improved heat dissipation, temperature roll-over at larger currents, increased output power, and increased cut-off frequency, as partly demonstrated for the first time in Figure 13. In comparison to a normal VCSEL, the new multi-aperture design, with ‘n’ number of apertures, will provide up to ‘n’ times the single-mode power at the same wavelength, while displaying smaller series resistance, a lower operating temperature of the active area, and a larger cut-off frequency.

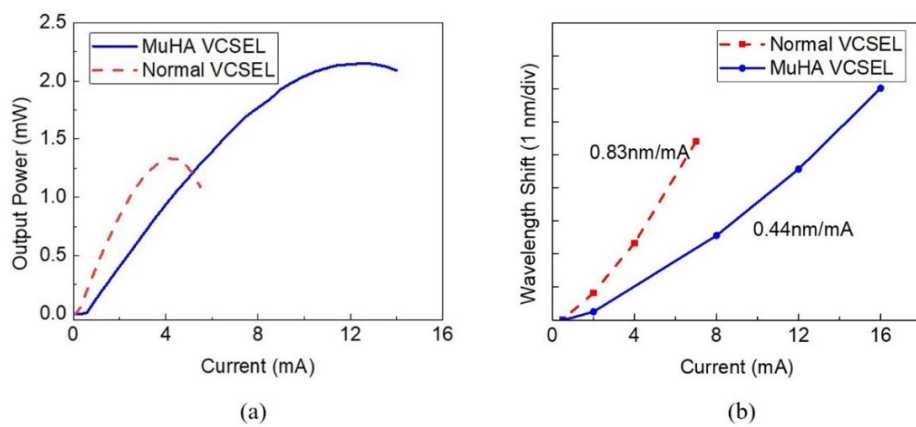


**Figure 13.** (a) Light-current of 940 nm normal VCSEL and 940 nm MuHA VCSEL. (b) The wavelength shifts of the normal VCSEL and the MuHA VCSEL. The oxide aperture areas of the two VCSELs are equal.

A technology of realizing compact coherently coupled VCSEL arrays by employing etched holes to oxidize AlAs-rich aperture layers was proposed [54,55]. Our goal is quite different: the reduction of the series resistance and largely improved heat dissipation. We fill the holes with an insulator and with metal. Our approach enables single aperture devices, multiple aperture devices at inter-aperture distances below the critical diameter of 50  $\mu\text{m}$  of classical multi-mode fibers, and polarized emissions. This approach presents an alternative manner of contacting the active area by bypassing most of the top mirror layers except for the last oxidized aperture and operates as an excellent heat sink, reducing the temperature of the active layer, and thus enabling larger currents and cut-off frequencies until a thermal turn-over is reached.

## 6. Conclusions and Outlooks

In this review, we have reviewed the success and limits of the present design of high-speed GaAs-based VCSELs with emission wavelengths from 850 nm to 1060 nm with an emphasis on energy efficiency. Larger modulation frequencies realized at smaller operating currents would be beneficial in lowering the energy consumption of high-speed VCSELs. Two approaches have been introduced to reduce energy consumption. First, photon lifetime management is emphasized as an approach to make classical VCSEL design adaptive to system demands. Second, a completely novel design approach based on oxide aperture formation from variable geometry holes etched in the wafer and filled with metal after etching is shown. A large improvement in the thermal properties, output power, cut-off frequency, and the energy consumption of devices, particularly with single mode emissions, are expected and realized for the first time. Several apertures can be combined into one device, additionally increasing single mode output power or allowing for polarization multiplexing.

For applications in optical interconnects, the VCSEL is integrated with driver integrated circuits (ICs) in a transmitter (Tx). Most of the power consumption of a VCSEL-based optical link occurs in the Tx and receiver (Rx) ICs. VCSEL-based optical links, capable of 55 Gbit/s operation, were demonstrated for 130 nm BiCMOS technology, and a total energy consumption of 1.25 W (738 mW Tx and + 512 mW Rx) was reported, corresponding to an energy consumption of 25 pJ/bit for the system at 55 Gb/s, and a low 250 fJ/bit for the VCSEL by itself [56]. VCSEL-based optical links capable of 71 Gbit/s operation were reported, showing a total energy consumption of 1.81 W (950 mW Tx and + 860 mW Rx), corresponding to an energy consumption of 25.5 pJ/bit [8]. VCSEL-based optical links (including Tx and Rx) capable of 56 Gbit/s and 72 Gbit/s operation were demonstrated in BiCMOS technology, with total energy consumptions of 4.5 pJ/bit [57] and 6.2 mW/Gbit [41], respectively. The use of power efficient ICs based on CMOS will enable VCSEL-based optical links with orders of magnitude lower energy consumption. The

development of new circuit technologies and the creation of new circuit architectures is presently under way and we expect that soon the power consumption of the drivers and the lasers will be similar to each other.

**Author Contributions:** Conceptualization, S.-C.T. and D.B.; writing—original draft preparation, S.-C.T.; writing—review and editing, M.A. and D.B.; supervision, D.B.; funding acquisition, S.-C.T. and D.B. All authors have read and agreed to the published version of the manuscript.

**Funding:** This work was partially supported by the National Key R&D Program of China (2021YFB2801000 and 2018YFB2201000), National Natural Science Foundation of China (62174159, 62061136010 and 62121005), Sino-German Center for Research Promotion (joint Mobility Program of DFG and NSFC M0386), Natural Science Foundation of Jilin Province (20210402055GH), and Chinese Academy of Sciences Youth Innovation Promotion Association (Y2022067).

**Institutional Review Board Statement:** Not applicable.

**Informed Consent Statement:** Not applicable.

**Data Availability Statement:** Not applicable.

**Acknowledgments:** We thank Gunter Larisch for fruitful discussions and his initial contributions.

**Conflicts of Interest:** The authors declare no conflict of interest.

## References

1. Global Internet Growth and Trends (Source: Cisco VNI Global IP Traffic Forecast, 2017–2022). Available online: <https://www.cisco.com/c/en/us/solutions/collateral/executive-perspectives/annual-internet-report/white-paper-c11-741490.pdf> (accessed on 9 March 2020).
2. Tian, S.-C.; Ahamed, M.; Larisch, G.; Bimberg, D. Novel energy-efficient designs of vertical-cavity surface emitting lasers for the next generations of photonic systems. *Jpn. J. Appl. Phys.* **2022**, *61*, SK0801. [[CrossRef](#)]
3. Iga, K. Surface-emitting laser—its birth and generation of new optoelectronics field. *IEEE J. Sel. Top. Quantum Electron.* **2000**, *6*, 1201–1215. [[CrossRef](#)]
4. Tatum, J.A.; Gazula, D.; Graham, L.A.; Guenter, J.K.; Johnson, R.H.; King, J.; Kocot, C.; Landry, G.D.; Lyubomirsky, I.; MacInnes, A.N.; et al. VCSEL-Based Interconnects for Current and Future Data Centers. *J. Light. Technol.* **2015**, *33*, 727–732. [[CrossRef](#)]
5. Mahgerefteh, D.; Thompson, C.; Cole, C.; Denoyer, G.; Nguyen, T.; Lyubomirsky, I.; Kocot, C.; Tatum, J. Techno-Economic Comparison of Silicon Photonics and Multimode VCSELs. *J. Light. Technol.* **2016**, *34*, 233–242. [[CrossRef](#)]
6. Moser, P.; Lott, J.A.; Larisch, G.; Bimberg, D. Impact of the Oxide-Aperture Diameter on the Energy Efficiency, Bandwidth, and Temperature Stability of 980-nm VCSELs. *J. Light. Technol.* **2015**, *33*, 825–831. [[CrossRef](#)]
7. Eiselt, N.; Griesser, H.; Wei, J.; Hohenleitner, R.; Dochhan, A.; Ortsiefer, M.; Eiselt, M.H.; Neumeyr, C.; Olmos, J.J.V.; Monroy, I.T. Experimental Demonstration of 84 Gb/s PAM-4 Over up to 1.6 km SSMF Using a 20-GHz VCSEL at 1525 nm. *J. Light. Technol.* **2017**, *35*, 1342–1349. [[CrossRef](#)]
8. Kuchta, D.M.; Rylyakov, A.V.; Doany, F.E.; Schow, C.L.; Proesel, J.E.; Baks, C.W.; Westbergh, P.; Gustavsson, J.S.; Larsson, A. A 71-Gb/s NRZ Modulated 850-nm VCSEL-Based Optical Link. *IEEE Photonics Technol. Lett.* **2015**, *27*, 577–580. [[CrossRef](#)]
9. Szczerba, K.; Westbergh, P.; Karlsson, M.; Andrekson, P.A.; Larsson, A. 70 Gbps 4-PAM and 56 Gbps 8-PAM Using an 850 nm VCSEL. *J. Light. Technol.* **2015**, *33*, 1395–1401. [[CrossRef](#)]
10. Larisch, G.; Rosales, R.; Bimberg, D. Energy-Efficient 50+ Gb/s VCSELs for 200+ Gb/s Optical Interconnects. *IEEE J. Sel. Top. Quantum Electron.* **2019**, *25*, 1701105. [[CrossRef](#)]
11. Moser, P.; Lott, J.A.; Wolf, P.; Larisch, G.; Li, H.; Ledentsov, N.N.; Bimberg, D. 56 fJ dissipated energy per bit of oxide-confined 850 nm VCSELs operating at 25 Gbit/s. *Electron. Lett.* **2012**, *48*, 1292–1294. [[CrossRef](#)]
12. Bimberg, D. Novel VCSEL Designs for the next generation of photonic systems. In Proceedings of the 2021 26th Microoptics Conference (MOC), Shizuoka, Japan, 26–29 September 2021; pp. 1–2.
13. Moser, P.; Hofmann, W.; Wolf, P.; Lott, J.A.; Larisch, G.; Payusov, A.; Ledentsov, N.N.; Bimberg, D. 81 fJ/bit energy-to-data ratio of 850 nm vertical-cavity surface-emitting lasers for optical interconnects. *Appl. Phys. Lett.* **2011**, *98*, 231106. [[CrossRef](#)]
14. Moser, P.; Lott, J.A.; Wolf, P.; Larisch, G.; Payusov, A.; Ledentsov, N.N.; Hofmann, W.; Bimberg, D. 99 fJ/(bit · km) Energy to Data-Distance Ratio at 17 Gb/s Across 1 km of Multimode Optical Fiber With 850-nm Single-Mode VCSELs. *IEEE Photonics Technol. Lett.* **2012**, *24*, 19–21. [[CrossRef](#)]
15. Coldren, L.A.; Corzine, S.W.; Mashanovitch, M.L. *Diode Lasers and Photonic Integrated Circuits*, 2nd ed.; Wiley: Hoboken, NJ, USA, 2012.
16. Larisch, G.; Moser, P.; Lott, J.A.; Bimberg, D. Impact of Photon Lifetime on the Temperature Stability of 50 Gb/s 980 nm VCSELs. *IEEE Photonics Technol. Lett.* **2016**, *28*, 2327–2330. [[CrossRef](#)]

17. Westbergh, P.; Gustavsson, J.S.; Kögel, B.; Haglund, Å.; Larsson, A. Impact of Photon Lifetime on High-Speed VCSEL Performance. *IEEE J. Sel. Top. Quantum Electron.* **2011**, *17*, 1603–1613. [[CrossRef](#)]
18. Westbergh, P.; Gustavsson, J.S.; Haglund, Å.; Skold, M.; Joel, A.; Larsson, A. High-Speed, Low-Current-Density 850 nm VCSELs. *IEEE J. Sel. Top. Quantum Electron.* **2009**, *15*, 694–703. [[CrossRef](#)]
19. Afromowitz, M.A. Thermal conductivity of Ga<sub>1-x</sub>Al<sub>x</sub>As alloys. *J. Appl. Phys.* **1973**, *44*, 1292–1294. [[CrossRef](#)]
20. Chang, Y.C.; Wang, C.S.; Johansson, L.A.; Coldren, L.A. High-efficiency, high-speed VCSELs with deep oxidation layers. *Electron. Lett.* **2006**, *42*, 1281–1283. [[CrossRef](#)]
21. Babichev, A.; Blokhin, S.; Gladyshev, A.; Karachinsky, L.; Novikov, I.; Blokhin, A.; Bobrov, M.; Maleev, N.; Andryushkin, V.; Kolodeznyi, E.; et al. Single-Mode High-Speed 1550 nm Wafer Fused VCSELs for Narrow WDM Systems. *IEEE Photonics Technol. Lett.* **2023**, *35*, 297–300. [[CrossRef](#)]
22. Babichev, A.V.; Karachinsky, L.Y.; Novikov, I.I.; Gladyshev, A.G.; Blokhin, S.A.; Mikhailov, S.; Iakovlev, V.; Sirbu, A.; Stepniak, G.; Chorchos, L.; et al. 6-mW Single-Mode High-Speed 1550-nm Wafer-Fused VCSELs for DWDM Application. *IEEE J. Quantum Electron.* **2017**, *53*, 2400808. [[CrossRef](#)]
23. Kapon, E.; Sirbu, A. Power-efficient answer. *Nat. Photonics* **2009**, *3*, 27–29. [[CrossRef](#)]
24. Blokhin, S.A.; Babichev, A.V.; Gladyshev, A.G.; Karachinsky, L.Y.; Novikov, I.I.; Blokhin, A.A.; Bobrov, M.A.; Maleev, N.A.; Andryushkin, V.V.; Denisov, D.V.; et al. High Power Single Mode 1300-nm Superlattice Based VCSEL: Impact of the Buried Tunnel Junction Diameter on Performance. *IEEE J. Quantum Electron.* **2022**, *58*, 2400115. [[CrossRef](#)]
25. Muller, M.; Hofmann, W.; Gründl, T.; Horn, M.; Wolf, P.; Nagel, R.D.; Ronneberg, E.; Bohm, G.; Bimberg, D.; Amann, M.C. 1550-nm High-Speed Short-Cavity VCSELs. *IEEE J. Sel. Top. Quantum Electron.* **2011**, *17*, 1158–1166. [[CrossRef](#)]
26. Sirbu, A.; Suruceanu, G.; Iakovlev, V.; Mereuta, A.; Mickovic, Z.; Caliman, A.; Kapon, E. Reliability of 1310 nm Wafer Fused VCSELs. *IEEE Photonics Technol. Lett.* **2013**, *25*, 1555–1558. [[CrossRef](#)]
27. Wolf, P.; Moser, P.; Larisch, G.; Hofmann, W.; Bimberg, D. High-Speed and Temperature-Stable, Oxide-Confining 980-nm VCSELs for Optical Interconnects. *IEEE J. Sel. Top. Quantum Electron.* **2013**, *19*, 1701207. [[CrossRef](#)]
28. Wolf, P.; Moser, P.; Larisch, G.; Li, H.; Lott, J.A.; Bimberg, D. Energy efficient 40 Gbit/s transmission with 850 nm VCSELs at 108 fJ/bit dissipated heat. *Electron. Lett.* **2013**, *49*, 666–667. [[CrossRef](#)]
29. Haglund, E.; Westbergh, P.; Gustavsson, J.S.; Haglund, E.P.; Larsson, A.; Geen, M.; Joel, A. 30 GHz bandwidth 850 nm VCSEL with sub-100 fJ/bit energy dissipation at 25–50 Gbit/s. *Electron. Lett.* **2015**, *51*, 1096–1098. [[CrossRef](#)]
30. Tan, F.; Wu, M.K.; Liu, M.; Feng, M.; Holonyak, N. 850 nm Oxide-VCSEL With Low Relative Intensity Noise and 40 Gb/s Error Free Data Transmission. *IEEE Photonics Technol. Lett.* **2014**, *26*, 289–292. [[CrossRef](#)]
31. Matsuo, S.; Sato, T.; Takeda, K.; Shinya, A.; Nozaki, K.; Taniyama, H.; Notomi, M.; Hasebe, K.; Kakitsuka, T. Ultralow Operating Energy Electrically Driven Photonic Crystal Lasers. *IEEE J. Sel. Top. Quantum Electron.* **2013**, *19*, 4900311. [[CrossRef](#)]
32. Li, H.; Wolf, P.; Moser, P.; Larisch, G.; Mutig, A.; Lott, J.A.; Bimberg, D. Energy-efficient and temperature-stable oxide-confined 980 nm VCSELs operating error-free at 38 Gbit/s at 85 degrees C. *Electron. Lett.* **2014**, *50*, 103–104. [[CrossRef](#)]
33. Moser, P.; Lott, J.A.; Wolf, P.; Larisch, G.; Li, H.; Bimberg, D. Error-free 46 Gbit/s operation of oxide-confined 980 nm VCSELs at 85 °C. *Electron. Lett.* **2014**, *50*, 1369–1371. [[CrossRef](#)]
34. Simpanen, E.; Gustavsson, J.S.; Haglund, E.P.; Larsson, A.; Sorin, W.V.; Mathai, S.; Tan, M.R. 1060 nm single-mode vertical-cavity surface-emitting laser operating at 50 Gbit/s data rate. *Electron. Lett.* **2017**, *53*, 869–871. [[CrossRef](#)]
35. Imai, S.; Takaki, K.; Kamiya, S.; Shimizu, H.; Yoshida, J.; Kawakita, Y.; Takagi, T.; Hiraiwa, K.; Shimizu, H.; Suzuki, T.; et al. Recorded Low Power Dissipation in Highly Reliable 1060-nm VCSELs for “Green” Optical Interconnection. *IEEE J. Sel. Top. Quantum Electron.* **2011**, *17*, 1614–1620. [[CrossRef](#)]
36. Müller, M.; Wolf, P.; Gründl, T.; Grasse, C.; Rosskopf, J.; Hofmann, W.; Bimberg, D.; Amann, M.C. Energy-efficient 1.3 μm short-cavity VCSELs for 30 Gb/s error-free optical links. In Proceedings of the ISLC 2012 International Semiconductor Laser Conference, San Diego, CA, USA, 7–10 October 2012; pp. 1–2.
37. Wolf, P.; Li, H.; Caliman, A.; Mereuta, A.; Iakovlev, V.; Sirbu, A.; Kapon, E.; Bimberg, D. Spectral Efficiency and Energy Efficiency of Pulse-Amplitude Modulation Using 1.3 μm Wafer-Fusion VCSELs for Optical Interconnects. *ACS Photonics* **2017**, *4*, 2018–2024. [[CrossRef](#)]
38. Spiga, S.; Soenen, W.; Andrejew, A.; Schoke, D.M.; Yin, X.; Bauwelinck, J.; Boehm, G.; Amann, M.C. Single-Mode High-Speed 1.5-μm VCSELs. *J. Light. Technol.* **2017**, *35*, 727–733. [[CrossRef](#)]
39. Tatum, J.A.; Landry, G.D.; Gazula, D.; Wade, J.K.; Westbergh, P. VCSEL-Based Optical Transceivers for Future Data Center Applications. In Proceedings of the Optical Fiber Communication Conference, San Diego, CA, USA, 11 March 2018; p. M3F.6.
40. Feng, M.; Wu, C.; Holonyak, N. Oxide-Confining VCSELs for High-Speed Optical Interconnects. *IEEE J. Quantum Electron.* **2018**, *54*, 2400115. [[CrossRef](#)]
41. Chorchos, L.; Ledentsov, N.; Kropp, J.R.; Shchukin, V.A.; Kalosha, V.P.; Lewandowski, A.; Turkiewicz, J.P.; Ledentsov, N.N. Energy Efficient 850 nm VCSEL Based Optical Transmitter and Receiver Link Capable of 80 Gbit/s NRZ Multi-Mode Fiber Data Transmission. *J. Light. Technol.* **2020**, *38*, 1747–1752. [[CrossRef](#)]
42. Moser, P.; Lott, J.A.; Bimberg, D. Energy Efficiency of Directly Modulated Oxide-Confining High Bit Rate 850-nm VCSELs for Optical Interconnects. *IEEE J. Sel. Top. Quantum Electron.* **2013**, *19*, 1702212. [[CrossRef](#)]
43. Li, H.; Wolf, P.; Moser, P.; Larisch, G.; Lott, J.; Bimberg, D. Vertical-cavity surface-emitting lasers for optical interconnects. *SPIE Newsroom* **2014**, *25*, 126103. [[CrossRef](#)]

44. Nasu, H. Short-Reach Optical Interconnects Employing High-Density Parallel-Optical Modules. *IEEE J. Sel. Top. Quantum Electron.* **2010**, *16*, 1337–1346. [[CrossRef](#)]
45. Chang, Y.-C.; Wang, C.S.; Coldren, L.A. High-efficiency, high-speed VCSELs with 35 Gbit/s error-free operation. *Electron. Lett.* **2007**, *43*, 1022–1023. [[CrossRef](#)]
46. Hatakeyama, H.; Akagawa, T.; Fukatsu, K.; Suzuki, N.; Tokutome, K.; Yashiki, K.; Anan, T.; Tsuji, M. 25 Gbit/s 100 °C operation of highly reliable InGaAs/GaAsP-VCSELs. *Electron. Lett.* **2009**, *45*, 45–46. [[CrossRef](#)]
47. Larisch, G.; Tian, S.; Bimberg, D. Optimization of VCSEL photon lifetime for minimum energy consumption at varying bit rates. *Opt. Express* **2020**, *28*, 18931–18937. [[CrossRef](#)] [[PubMed](#)]
48. Li, H.; Wolf, P.; Moser, P.; Larisch, G.; Mutig, A.; Lott, J.A.; Bimberg, D.H. Impact of the Quantum Well Gain-to-Cavity Etalon Wavelength Offset on the High Temperature Performance of High Bit Rate 980-nm VCSELs. *IEEE J. Quantum Electron.* **2014**, *50*, 613–621. [[CrossRef](#)]
49. Larisch, G.; Tian, S.C.; Bimberg, D. "Radiation Emitter". US 17 327 328, 14 April 2021.
50. Larisch, G.; Tian, S.C.; Bimberg, D. "Radiation Emitter". EP 21 168 265.3, 14 April 2020.
51. Larisch, G.; Tian, S.C.; Bimberg, D. "Radiation Emitter". US 17 170 834, 8 February 2021.
52. Larisch, G.; Tian, S.C.; Bimberg, D. "Radiation Emitter". EP 20 192 355.4, 24 August 2020.
53. Mansoor, A.; Tian, S.C.; Lindner, J.; Larisch, G.; Bimberg, D. Multi-aperture VCSELs: High power, low resistance, single mode. In Proceedings of the 2021 27th International Semiconductor Laser Conference (ISLC), Potsdam, Germany, 10–14 October 2021; pp. 1–2.
54. Chua, C.L.; Thornton, R.L.; Treat, D.W. Method and Structure for Eliminating Polarization Instability in Laterally-Oxidized VCSELs. US 6 304 588, 2 September 1999.
55. Chua, C.L. "Phase Array Oxide-Confined VCSELs". US 7 257 141, 23 July 2003.
56. Kuchta, D.M.; Rylyakov, A.V.; Schow, C.L.; Proesel, J.E.; Baks, C.; Kocot, C.; Graham, L.; Johnson, R.; Landry, G.; Shaw, E.; et al. A 55Gb/s directly modulated 850nm VCSEL-based optical link. In Proceedings of the IEEE Photonics Conference 2012, Burlingame, CA, USA, 23–27 September 2012; p. 972.
57. Ledentsov, N., Jr.; Agustin, M.; Chorchos, L.; Kropp, J.-R.; Shchukin, V.; Kalosha, V.; Koepp, M.; Caspar, C.; Turkiewicz, J.; Ledentsov, N. *Energy Efficient 850-nm VCSEL Based Optical Transmitter and Receiver Link Capable of 56 Gbit/s NRZ Operation*; SPIE: Pontoise, France, 2019; Volume 10938.

**Disclaimer/Publisher's Note:** The statements, opinions and data contained in all publications are solely those of the individual author(s) and contributor(s) and not of MDPI and/or the editor(s). MDPI and/or the editor(s) disclaim responsibility for any injury to people or property resulting from any ideas, methods, instructions or products referred to in the content.